

# Tracking Control of Direct-Drive Servos

Sergey Edward Lyshevski<sup>1</sup> and Trevor C. Smith<sup>2</sup>

<sup>1</sup>Department of Electrical and Microelectronic Engineering  
Rochester Institute of Technology, Rochester, New York 14623-5603, USA

<sup>2</sup>Harris Corporation, Rochester, NY 14618, USA

E-mail: [Sergey.Lyshevski@mail.rit.edu](mailto:Sergey.Lyshevski@mail.rit.edu) Web: <http://people.rit.edu/seleeec/>

**Abstract** – Multi-objective optimization, data-intensive analysis and hardware-software co-design are the major challenging themes in the concurrent design of high-performance electromechanical systems. Direct-drive servos guarantee superior torque and force densities, efficiency, robustness, simplicity and other enabling performance quantities. Nano-, micro-, mini- and macro-scale axial and radial actuators exist in a great variety, e.g., from living organisms to various *engineered* electromechanical systems. Permanent-magnet actuators and servos are widely used in aerospace, automotive, biotechnology, energy, medical, power, robotic and other applications. The major goal of this paper is to report and apply advanced concepts in design and implementation of tracking control laws. These control laws are designed using the state transformation method applying the Hamilton-Jacobi optimization and Lyapunov stability theory. We design and evaluate high-performance drives and servos. Various servo-systems with radial- and axial-topology actuators are demonstrated and characterized by evaluating analog and digital tracking control laws. The studied direct-drive actuators with SmCo permanent-magnet arrays guarantee high torque density, high efficiency, reliability, fast dynamics, etc. The controllers designed guarantee stability, high precision and robustness. The high-frequency PWM drivers vary the voltage applied by changing the duty ratio of FETs. High-accuracy sensors measure angular velocity and displacement. Linear and nonlinear analog control laws guarantee superior performance, enabling capabilities, minimal complexity, simplicity, noise immunity, etc. The analog control laws can be discretized and implemented using microcontrollers and DSPs. The studied drives and servos are applicable in many applications, including hard drives, high-precision pointing systems, rotating tables, manipulators, etc. This paper examines and solves a spectrum of pertinent problems in design and implementation of enabling minimal-complexity control laws and controllers which guarantee near-optimal system performance

## I. INTRODUCTION

Various nonlinear analysis, control and optimization concepts have been used in design of electromechanical systems. In high-performance drives, servos, additional factors and considerations emerged due to the strengthening of performance requirements, hardware limits, etc. These high-performance direct-drive actuators with matching sensors and ICs must ensure *minimal complexity* while guaranteeing optimal performance and capabilities.

Control laws must be designed and implemented with the ultimate goal to optimize overall dynamic performance (stability, accuracy, settling time, robustness, etc.), improve operating characteristics, enhance operating envelopes, etc.

Design of *minimal complexity* closed-loop systems is the key to attaining desired performance. Though various control methods were proposed in [1-5] and references therein, their overall applicability, suitability and practicality must be examined. Control schemes are actuator-specific. Operating principles and control algorithms for various classes of electrostatic and electromagnetic actuators are fundamentally distinct. Design of control laws and their consequent implementation have not been sufficiently studied. Application of many concepts, which were applied to descriptive *generic* models of dynamic systems, may not guarantee the desired performance, specified capabilities, required adaptability and overall practicality [6, 7]. For example, adaptive, “intelligent” and other control schemes require advanced DSPs to ensure real-time decision-making, reconfiguration, etc. Correspondingly, the overall practicality and other factors suggest one to focus on practical solutions. As illustrated in Figure 1, the dimensionality of actuators may be less than operational amplifiers and sensors. Controlling electronics and ASICs should be designed to reduce hardware complexity with a minimum number of measured variables and feedback.



Figure 1. Mini-motors with ASICs: Actuators are fabricated utilizing *bulk* and surface micromachining technologies [7]

Linear and nonlinear proportional-integral-derivative (PID) control laws, linear quadratic algorithms, nonlinear compensators and *soft-switching* sliding mode control schemes have been widely used for decades in MIMO electromechanical systems, robots, flight/ground/marine vehicles, etc. The aforementioned control schemes usually ensure near-optimal performance. These control laws are designed using the Hamilton-Jacobi theory, Lyapunov stability concepts and other methods [6-8]. However, some deficiencies may emerge in the design of minimal complexity systems with strict performance requirements in the expanded operating envelope. The aforementioned challenges necessitate design of robust tracking proportional-integral control laws with state feedback. We

design, demonstrate, test and characterize high-performance drives and servos with advanced hardware solutions and control schemes. This paper considers two general classes of servos which guarantee:

1. Bidirectional 360-degree-of-rotation;
2. Bidirectional limited-angle displacement.

In these drives and servos, many-pole radial- and axial topology actuators are used. These high-torque-density permanent-magnet actuators are controlled by high-switching-frequency PWM *drivers* which change the applied voltage. Excellent performance and enabling capabilities are achieved by using high-performance actuators, power electronic *drivers* with two- and four-quadrant power stages, sensors, and other components. The control laws are designed to satisfy the specifications imposed, e.g., stability, minimal settling time, high acceleration, accuracy, disturbance attenuation, robustness to parameter variations, minimal complexity, practicality, etc.

Axial topology permanent-magnet actuators are documented in Figure 2. Fully integrated direct-drive actuators and servos are built, tested and characterized. A servo-system with a limited-angle axial-topology actuator is depicted in Figure 3. The reference signal is the angular displacement. Using the reference  $\theta_{ref}$  and actual  $\theta_r$  angular displacements (measured by the high-accuracy sensor), the controller ICs drive the comparator, changing the switching activity of output stage FETs. Hence, the voltage  $u_a$  applied to the winding varies [7].

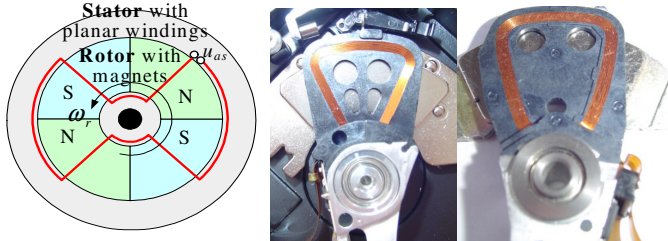


Figure 2. Single-phase axial topology actuator. Images of axial-topology hard-drive: Rotor (pointer) with planar deposited coils above a stator aperture with SmCo permanent magnets [7]

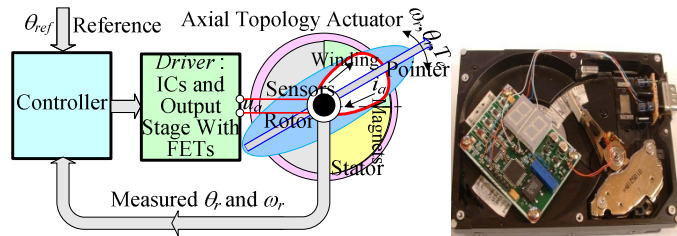


Figure 3. Closed-loop servo: Actuator (Pointer) – Sensors – PWM Driver (ICs, output stage and other circuitry) - Controller

Our basic, analytic and experimental developments unify nonlinear design, analysis and implementation. We report the systematic procedures in the design of tracking control laws. Experiments are reported to assess closed-loop servos evaluating dynamic and steady-state performance, as well as overall capabilities.

## II. MODELS OF PERMANENT-MAGNET SERVOMOTORS

We examine bidirectional 360-degree-of-rotation and limited-angle actuators. These radial- and axial topology actuators are designed within single-, two- and three-phase *ac/dc* electromagnetics and electric machine configurations. High-fidelity mathematical models are developed in [7]. In general, the *circuitry-electromagnetic* and *torsional-mechanical* equations of motion are

$$\mathbf{u} = \mathbf{r}_s \mathbf{i} + \frac{d\boldsymbol{\Psi}}{dt}, \quad J\boldsymbol{\alpha} = \Sigma \mathbf{T}, \quad (1)$$

where  $\mathbf{u}$  and  $\mathbf{i}$  are the vector of the applied voltages and phase currents (for single- and three-phase actuators,  $\mathbf{u}=u_a$ ,  $\mathbf{i}=i_a$  and  $\mathbf{u}=[u_{as} \ u_{bs} \ u_{cs}]^T$ ,  $\mathbf{i}=[i_{as} \ i_{bs} \ i_{cs}]^T$ );  $\mathbf{r}_s$  is the phase resistance;  $\boldsymbol{\Psi}$  is the vector of flux linkages;  $\boldsymbol{\alpha}$  is the angular acceleration;  $\Sigma \mathbf{T}$  is the *net* torque;  $J$  is the equivalent moment of inertia.

For the one-dimensional case, assuming that the friction torque is  $B_m \omega_r$ , the *torsional-mechanical* dynamics  $J\boldsymbol{\alpha} = \Sigma \mathbf{T}$  leads to

$$\frac{d^2 \theta_r}{dt^2} = \frac{1}{J} (T_e - B_m \omega_r - \Sigma T_L),$$

$$\text{or, } \frac{d\omega_r}{dt} = \frac{1}{J} (T_e - B_m \omega_r - \Sigma T_L), \quad \frac{d\theta_r}{dt} = \omega_r, \quad (2)$$

where  $B_m$  is the friction coefficient;  $T_e$  is the electromagnetic torque;  $\Sigma T_L$  is the *net* load, perturbation, disturbance and other torques.

### 2. 1. Direct-Drive Limited-Angle Actuators

Consider a bidirectional direct-drive axial topology actuator with a segmented array of permanent magnets as documented in Figure 2. These high-torque-density permanent-magnet actuators exceed performance and capabilities achieved by other servo-motors [7]. The electromagnetic design and optimization of the aforementioned actuators are reported in [7].

The mathematical model is found to perform numerical analysis and design of control laws. Depending on the magnetization, the magnetic field developed by the magnets is approximated as continuous or discontinuous functions. For limited-angle actuators, which are shown in Figures 2 and 3, depending on the geometry, structural design, magnetization and separations of magnets, one has

$$B(\theta_r) = a \theta_r, \quad |B(\theta_r)| \leq B_{\max},$$

$$B(\theta_r) = B_{\max} \sin^{2q-1}(a \theta_r), \quad \text{or } B(\theta_r) = B_{\max} \tanh^{2q-1}(a \theta_r),$$

where  $B_{\max}$  is the magnetic flux density from the permanent magnets as viewed at the coils;  $a$  is the magnetization, technology- and size-dependent constant;  $q$  is the technology-dependent integer, and, usually  $q=1$  or  $q=2$ .

The magnetic coupling between the current loop (winding) and segmented permanent magnets leads to the electromagnetic torque. The electromagnetic torque can be derived using the magnetic dipole moment  $\mathbf{m}$ ,  $\mathbf{T}_e = \mathbf{m} \times \mathbf{B}$ . For a straight filament (conductor) in a uniform magnetic field

$$\mathbf{F} = i \mathbf{l} \times \mathbf{B}, \quad \mathbf{F} = -i \mathbf{B} \times d\mathbf{l}. \quad (3)$$

We assume optimal electromagnetic and mechanical designs. The electromagnetic forces  $F_{eL}$  and  $F_{eR}$  are developed by the right and left filaments. Thus,

$$T_e = T_{eL} + T_{eR} = R_{\perp} \Sigma F = R_{\perp} (F_{eL} + F_{eR}), \quad (4)$$

where  $R_{\perp}$  is the perpendicular radius.

*Example 2. 1.* Let  $B(\theta_r) = B_{\max} \tanh^{2q-1}(a\theta_r)$ ,  $q=1$ ,  $a \gg 1$ .

From  $\tanh(a\theta_r) \approx 1$  and  $\tanh(a\theta_L) \approx 1$  ( $\theta_r \neq 0$  and  $\theta_L \neq 0$ ), one finds the expression for the electromagnetic torque

$$T_{e_i} = T_{eL} + T_{eR} = 2R_{\perp} l_{eq} N B_{\max} i_a,$$

where  $\theta_R$  and  $\theta_L$  are the relative angular displacements of the right and left filaments;  $N$  is the number turns in filaments;  $l_{eq}$  is the coil *effective* active length;  $i_a$  is the current in the coil. ■

The mathematical model is found by using Kirchhoff's and Newton's second laws [7]. The *circuitry-electromagnetic* and *torsional-mechanical* equations (1) are

$$u_a = r_s i_a + \frac{d\psi}{dt}, \quad \frac{d^2\theta_r}{dt^2} = \frac{1}{J} (T_e - B_m \omega_r - \Sigma T_L). \quad (5)$$

The expression for the induced *emf* is

$$\mathcal{E} = \oint_l \vec{E}(t) \cdot d\vec{l} = -\frac{d}{dt} \int_s \vec{B}(t) \cdot d\vec{s} = -N \frac{d\Phi}{dt} = -\frac{d\psi}{dt}. \quad (6)$$

*Example 2. 2.* Consider a typical magnetization with  $B(\theta_r) = B_{\max} \tanh(a\theta_r)$ .

From  $\mathcal{E} = -N \frac{d}{dt} \int_{r_{\min}}^{r_{\max}} \int_{\theta_{\min}}^{\theta_{\max}} B_{\max} \tanh(a\theta_r) r dr d\theta_r$ , one finds

$$\mathcal{E} = -\frac{r_{out}^2 - r_{in}^2}{2} N B_{\max} (\tanh a\theta_L + \tanh a\theta_R) \omega_r, \quad (7)$$

where  $\theta_L(t) = \theta_{L0} - \theta_r(t)$  and  $\theta_R(t) = \theta_{R0} + \theta_r(t)$ ;  $\theta_{L0} = \theta_{R0} = \theta_{r\max}$ .

From (5), a set of nonlinear differential equations which describes the dynamics of a limited-angle axial-topology actuator is

$$\begin{aligned} \frac{di_a}{dt} &= \frac{1}{L_a} \left[ -r_a i_a - \frac{r_{out}^2 - r_{in}^2}{2} N B_{\max} (\tanh a\theta_L + \tanh a\theta_R) \omega_r + u_a \right], \\ \frac{d\omega_r}{dt} &= \frac{1}{J} \left[ R_{\perp} l_{eq} N B_{\max} (\tanh a\theta_L + \tanh a\theta_R) i_a - B_m \omega_r - T_s - T_{\xi} \right], \\ \frac{d\theta_r}{dt} &= \omega_r, \quad -\theta_{r\max} \leq \theta_r \leq \theta_{r\max}, \end{aligned} \quad (8)$$

where  $L_a$  is the self-inductance;  $T_s$  is the restoring force,  $T_s = k_{s1} \theta_r + k_{s3} \theta_r^3$ ;  $k_{s1}$  and  $k_{s3}$  are the restoring constants (spring, permanent magnet and other schemes are used);  $T_{\xi}$  is the stochastic torque (perturbations and disturbances). ■

The winding resistance  $r_s$  varies due to temperature changes. The friction coefficient  $B_m$  can vary due to mechanical wearing, bending, changes of the operating envelope, etc. The equivalent moment of inertia  $J$  may vary. These parameter variations are accounted [7].

## 2. 2. Radial and Axial Topology Actuators

The mathematical models of rotational radial- and axial topology two- and three-phase actuators are found utilizing differential equations (1). The electromagnetic design, magnetization and magnet placement define the coupling

magnetic field  $B(\theta_r)$ . One derives the resulting expressions for the *emf*  $\mathcal{E}$  and electromagnetic torque  $T_e$  [6, 7].

*Example 2. 3.* For a single-phase axial-topology permanent-magnet motor one may have

$B(\theta_r) = B_{\max} \sin^{2q-1}(\frac{1}{2} N_m \theta_r)$  or  $B(\theta_r) = B_{\max} \text{sgn}[\sin(\frac{1}{2} N_m \theta_r)]$ , where  $N_m$  is the number of magnets.

Using the electrical angular displacement  $\theta_r$ , for two- and three-phase permanent magnet synchronous machines with ( $as$  and  $bs$ ) and ( $as$ ,  $bs$  and  $cs$ ) windings, we have

$$\begin{aligned} B_{as}(\theta_r) &= B_{\max} \sin^{2q-1}(\theta_r) \text{ and } B_{bs}(\theta_r) = B_{\max} \cos^{2q-1}(\theta_r), \\ \text{and } B_{as}(\theta_r) &= B_{\max} \sin^{2q-1}(\theta_r), \quad B_{bs}(\theta_r) = B_{\max} \sin^{2q-1}(\theta_r - \frac{2}{3}\pi), \\ B_{cs}(\theta_r) &= B_{\max} \sin^{2q-1}(\theta_r + \frac{2}{3}\pi). \end{aligned}$$

The resulting electromagnetic design and equations of motion are straightforward to carry-out. ■

## III. CONTROL OF SERVO-SYSTEMS

The differential equations (1) are nonlinear. Furthermore, for rotational radial- and axial topology two- and three-phase actuators, the applied voltages must be applied as a function of the rotor angular displacement  $\theta_r$ . The magnitude of the applied PWM voltage  $u_m$  is bounded. The FETs duty cycle  $d_D$  is bounded as  $-1 \leq d_D \leq 1$ . Thus,  $u_{\min} \leq u \leq u_{\max}$ . To control the applied voltage, we use the signal-level control voltage  $u_c$  supplied to the comparator thereby defining the duty ratio of the FETs [7]. High-performance *drivers* with two- and four-quadrant power stages and different switching configurations are used to vary the applied voltage supplied to the phase windings.

The transient dynamics of ICs and power electronic circuitry are within the nanosecond range. These fast dynamics and parameter variations can be accounted as bounded uncertainties  $p \in P$ . The studied servo is modeled as

$$\dot{x}^{\text{sys}}(t) = F(p, x^{\text{sys}}) + B(p, x^{\text{sys}})u, \quad y = Hx^{\text{sys}}, \quad (9)$$

where  $x^{\text{sys}} \in X^{\text{sys}} \subset \mathbb{R}^n$  is the state vector;  $u \in U \subset \mathbb{R}^m$  is the control vector;  $y \in Y \subset \mathbb{R}^b$  is the output vector;  $F(\cdot, \cdot)$  and  $B(\cdot, \cdot)$  are the smooth Lipschitz maps;  $H \in \mathbb{R}^{b \times c}$  is the output matrix with constant coefficients.

### 3.1. Design of Tracking Proportional-Integral Control Laws With State Feedback: Unconstrained Control

Consider the following model

$$\dot{x}^{\text{sys}}(t) = A^{\text{sys}} x^{\text{sys}} + B^{\text{sys}} u, \quad y = Hx^{\text{sys}}, \quad (10)$$

where  $A^{\text{sys}} \in \mathbb{R}^{n \times n}$  and  $B^{\text{sys}} \in \mathbb{R}^{n \times m}$  are the constant-coefficient matrices.

*Example 3. 1.* For the limited-angle servos, depending on permanent magnet magnetization, the governing equations of motion are derived. Consider the resulting model (8) which corresponds to  $B(\theta_r) = B_{\max} \tanh(a\theta_r)$ . To maximize the torque, magnets are magnetized such that  $a \gg 1$ . One finds

$$\mathcal{E} \approx -k_a \omega_r,$$

where  $k_a$  is the *back emf* constant.

From  $T_e = T_{eL} + T_{eR} = R_{\perp} l_{eq} N B_{\max} (\tanh a\theta_L + \tanh a\theta_R) i_a$ , we have  $T_e \approx 2R_{\perp} l_{eq} N B_{\max} i_a$ .

Thus, the equations of motion (8) are simplified to

$$\begin{aligned}\frac{di_a}{dt} &= \frac{1}{L_a}(-r_a i_a - k_a \omega_r + u_a), \\ \frac{d\omega_r}{dt} &= \frac{1}{J} [2R_{\perp} l_{eq} N B_{\max} i_a - B_m \omega_r - k_s \theta_r - T_{\xi}], \\ \frac{d\theta_r}{dt} &= \omega_r, \quad -\theta_{r\max} \leq \theta_r \leq \theta_{r\max}.\end{aligned}$$

That is, linear differential equations (10) result. ■

The tracking error vector  $e \in \mathbb{R}^b$  is

$$e(t) = Nr(t) - y(t) = Nr(t) - Hx^{\text{sys}}(t). \quad (11)$$

To enable stability of the tracking error evolution, we define the evolution of  $de/dt$  as

$$\dot{e}(t) = -I_E e - HA^{\text{sys}} x^{\text{sys}} - HB^{\text{sys}} u, \quad (12)$$

where  $I_E \in \mathbb{R}^{b \times b}$  is the identity matrix.

Using the expanded vector  $x = [x^{\text{sys}} \ e]^T$ , we have

$$\dot{x}(t) = \begin{bmatrix} \dot{x}^{\text{sys}}(t) \\ \dot{e}(t) \end{bmatrix} = \begin{bmatrix} A^{\text{sys}} & 0 \\ -HA^{\text{sys}} & -I_E \end{bmatrix} \begin{bmatrix} x^{\text{sys}} \\ e \end{bmatrix} + \begin{bmatrix} B^{\text{sys}} \\ -HB^{\text{sys}} \end{bmatrix} u = Ax + Bu. \quad (13)$$

The *space transformation* method [6, 7] uses vectors

$$z = \begin{bmatrix} x \\ u \end{bmatrix}, \quad z \in \mathbb{R}^{n+b+m} \quad \text{and} \quad v = \dot{u}, \quad v \in \mathbb{R}^m \quad (14)$$

We define the variables as

$$z = \begin{bmatrix} x \\ u \end{bmatrix}, \quad z \in \mathbb{R}^{n+b+m} \quad \text{and} \quad v = \dot{u} + u, \quad v \in \mathbb{R}^m. \quad (15)$$

The evolution of the control function is governed by the following equation

$$\dot{u} = -I_U u + I_U v, \quad (16)$$

where  $I_U \in \mathbb{R}^{m \times m}$  is the identity matrix.

From (10)-(16), one obtains the system

$$\dot{z}(t) = \begin{bmatrix} A & B \\ 0 & -I_U \end{bmatrix} z + \begin{bmatrix} 0 \\ I_U \end{bmatrix} v = A_z z + B_z v, \quad y = Hx^{\text{sys}}. \quad (17)$$

*Design Problem Formulation:* Minimize the quadratic performance functional

$$J = \int_{t_0}^{t_f} (z^T Q_z z + v^T G_z v) dt, \quad (18)$$

subject to the system dynamics (17). □

In (18),  $Q_z \in \mathbb{R}^{(n+b+m) \times (n+b+m)}$ ,  $Q_z \geq 0$ ,  $G_z \in \mathbb{R}^{m \times m}$ ,  $G_z > 0$ .

The Hamilton-Jacobi principle is applied. The first-order necessary condition for optimality  $\partial H/\partial v = 0$  gives

$$v = -G_z^{-1} B_z^T K_z z. \quad (19)$$

The Riccati equation

$$-\dot{K} = KA_z + A_z^T K - KB_z G_z^{-1} B_z^T K + Q_z, \quad K(t_f) = K_f \quad (20)$$

is solved to find the unknown matrix  $K \in \mathbb{R}^{(n+b+m) \times (n+b+m)}$ .

From (16) and (19), one has

$$\begin{aligned}\dot{u}(t) &= -G_z^{-1} B_z^T K_z z - I_U u = -G_z^{-1} \begin{bmatrix} 0 \\ I_U \end{bmatrix}^T \begin{bmatrix} K_{11} & K_{21}^T \\ K_{21} & K_{22} \end{bmatrix} \begin{bmatrix} x \\ u \end{bmatrix} - I_U u \quad (21) \\ &= -G_z^{-1} K_{21} x - (G_z^{-1} K_{22} + I_U) u = K_{f1} x + K_{f2} u.\end{aligned}$$

From  $\dot{x}(t) = Ax + Bu$ ,  $u = B^{-1}(\dot{x}(t) - Ax) = (B^T B)^{-1} B^T (\dot{x}(t) - Ax)$

Therefore, using (21), one obtains

$$\begin{aligned}\dot{u}(t) &= K_{f1} x + K_{f2} u = K_{f1} x + K_{f2} (B^T B)^{-1} B^T (\dot{x}(t) - Ax) \\ &= \left[ K_{f1} - K_{f2} (B^T B)^{-1} B^T A \right] x(t) + K_{f2} (B^T B)^{-1} B^T \dot{x}(t) \quad (22) \\ &= (K_{f1} - K_{f1} A) x(t) + K_{f1} \dot{x}(t) = K_{F2} x(t) + K_{F1} \dot{x}(t).\end{aligned}$$

From (22) and recalling that  $x(t) = \begin{bmatrix} x^{\text{sys}}(t) \\ e(t) \end{bmatrix}$ , one finds

an optimal proportional-integral control law with state feedback. In particular,

$$\begin{aligned}u(t) &= K_{F1} x(t) - K_{F1} x_0 + \int K_{F2} x(\tau) d\tau + u_0 \\ &= K_{F1} \begin{bmatrix} x^{\text{sys}}(t) \\ e(t) \end{bmatrix} - K_{F1} \begin{bmatrix} x_0^{\text{sys}}(t) \\ e_0(t) \end{bmatrix} + \int K_{F2} \begin{bmatrix} x^{\text{sys}}(\tau) \\ e(\tau) \end{bmatrix} d\tau + u_0.\end{aligned} \quad (23)$$

For nonlinear systems (9), the proposed procedure can be straightforwardly used. One finds the proportional-integral control law with state feedback as

$$\dot{u}(t) = -G_z^{-1} B_z^T \frac{\partial V}{\partial z} - I_U u = -G_z^{-1} \begin{bmatrix} 0 \\ I_U \end{bmatrix}^T \frac{\partial V(x, u)}{\partial [x u]^T} - I_U u, \quad (24)$$

where  $V(x, u)$  is the return function.

*Example 3. 2.*

Consider the so-called *force/torque* control problem. We examine the second-order translational- or rotational dynamics of mechanical systems which are modeled as

$$\frac{dx_1}{dt} = -x_1 + u, \quad \frac{dx_2}{dt} = x_1, \quad y = x_2. \quad (25)$$

Here,  $x_1$  and  $x_2$  are the linear (angular) velocity and displacement;  $u$  is the control (force or torque).

The PID control law

$$u = k_p e + k_i \int e dt + k_d de/dt, \quad (26)$$

is synthesized to be

$$u = 100e + 10de/dt, \quad e = r - x_2. \quad (27)$$

Using the state-transformation method, one obtains

$$A_z = \begin{bmatrix} -1 & 0 & 0 & 1 \\ 1 & 0 & 0 & 0 \\ -1 & 0 & -1 & 0 \\ 0 & 0 & 0 & -1 \end{bmatrix} \quad \text{and} \quad B_z = \begin{bmatrix} 0 \\ 0 \\ 0 \\ 1 \end{bmatrix}. \quad \text{Let} \quad Q_z = \begin{bmatrix} 1 & 0 & 0 & 0 \\ 0 & 1 & 0 & 0 \\ 0 & 0 & 100000 & 0 \\ 0 & 0 & 0 & 1 \end{bmatrix} \quad \text{and}$$

$G_z = 1$ . From (23) one has

$$u(t) = K_{F1} x(t) + \int K_{F2} x(\tau) d\tau = K_{F1} \begin{bmatrix} x_1 \\ x_2 \\ e \end{bmatrix} + K_{F2} \int \begin{bmatrix} x_1 \\ x_2 \\ e \end{bmatrix} d\tau \quad (28)$$

The following feedback matrices are found

$$K_{F1} = [-11.83 \ 0 \ 0] \quad \text{and} \quad K_{F2} = [-80.75 \ -1 \ -234.78].$$

Figure 4 reports the simulation results for linear closed-loop systems (25)-(27) and (25)-(28) if the reference signal is  $r = \pm 1$ . The evolution of the output  $y = x_2$  is of our particular interest. Control law (28) ensures better closed-loop system performance than compared with PID control (26).

In electromechanical, electronic, mechanical and other systems, there are limits on *control efforts*. That is, due to mechanical, electromagnetic and other physical limits, control  $u$  is constrained as  $u_{\min} \leq u \leq u_{\max}$ .

Thus, we have control laws with bounds, and

$$u = k_p e + k_i \int e dt + k_d de/dt, \quad u_{\min} \leq u \leq u_{\max}, \quad (29)$$

$$u(t) = K_{F1} \begin{bmatrix} x_1 \\ x_2 \\ e \end{bmatrix} + K_{F2} \int \begin{bmatrix} x_1 \\ x_2 \\ e \end{bmatrix} d\tau, \quad u_{\min} \leq u \leq u_{\max}. \quad (30)$$

For  $-20 \leq u \leq 20$ , the simulations of system (25) with control laws (29) and (30) are documented in Figure 5.

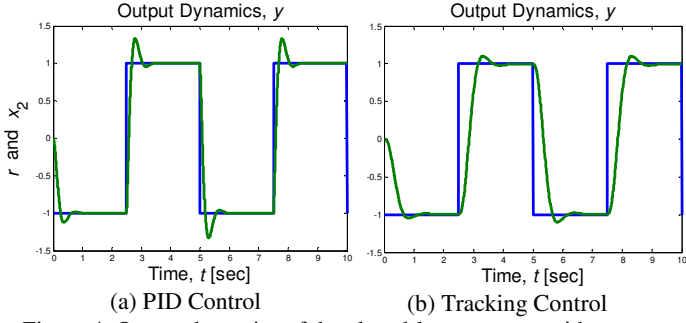


Figure 4. Output dynamics of the closed-loop systems with: (a) Proportional-derivative control law; (b) Tracking control law.

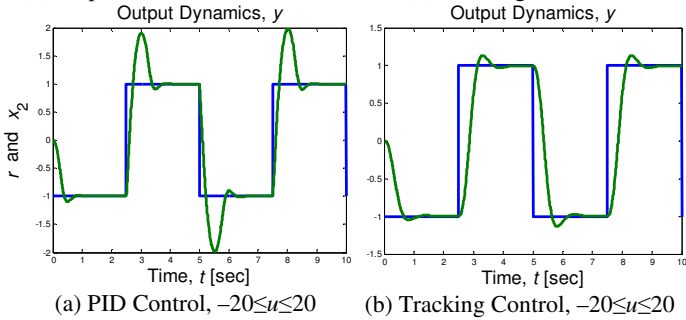


Figure 5. Output dynamics of the closed-loop systems with control bounds  $-20 \leq u \leq 20$ : (a) Proportional-derivative control law; (b) Tracking control law.

If the amplitude of the reference signal  $r(t)$  increases, the closed-loop system with a bounded PID control law (29) becomes unstable. In contrast, the tracking control law with state feedback (30) guarantees stability and robustness in the expanded envelopes  $XE$  despite control bounds. ■

### 3.2. Constrained Control

The control law is bounded as  $u_{\min} \leq u \leq u_{\max}$ . To design the *admissible* control laws, we minimize [6-10]

$$J = \int_{t_0}^{t_f} \left[ x^T Q x + \int (\Phi^{-1}(u))^T G du \right] dt, \quad (31)$$

where  $\Phi(\cdot): \mathbb{R}^{n+b} \rightarrow \mathbb{R}^m$  is the bounded, integrable, one-to-one, real-analytic globally Lipschitz continuous function,  $\Phi \in U \subset \mathbb{R}^m$ .

Minimizing (31), for linear and nonlinear systems with  $u_{\min} \leq u \leq u_{\max}$ ,  $u \in U$ , we have

$$-\frac{\partial V}{\partial t} = \min_{u \in U} \left\{ x^T Q x + \int (\Phi^{-1}(u))^T G du + \frac{\partial V^T}{\partial z} (Ax + Bu) \right\}, \quad (32)$$

and

$$-\frac{\partial V}{\partial t} = \min_{u \in U} \left\{ x^T Q x + \int (\Phi^{-1}(u))^T G du + \frac{\partial V^T}{\partial z} [F(x) + B(x)u] \right\} \quad (33)$$

Using the first-order necessary condition for optimality, an *admissible* control law is found to be [6-10]

$$u(t) = -\Phi \left( G^{-1} B^T \frac{\partial V}{\partial x} \right), \quad u \in U. \quad (34)$$

The solution of the Hamilton-Jacobi equation is approximated by the quadratic or non-quadratic return function. One obtains control laws with linear and nonlinear switching surfaces, respectively. The *admissible* control law (34) is bounded. The second-order necessary condition for optimality is satisfied. However, the sufficient conditions must be examined. The *admissibility* concept is applied [8].

Applying the state transformation method and using the quadratic return function, one obtains

$$u(t) = \Phi \left( K_{F1} x(t) + \int K_{F2} x(\tau) d\tau \right), \quad u \in U. \quad (35)$$

**Theorem 3. 1.** A closed-loop system with a bounded control law  $u \in U$  (35) is robustly stable in  $X(X_0, U, P)$ , and, robust tracking is guaranteed in the convex and compact set  $E(E_0, Y, R)$ , if for the reference input  $r \in R$  and uncertainties (parameter variations, unmodeled dynamics, etc.)  $p \in P$ , there exists a  $C^k$  ( $k \geq 1$ ) positive-definite function  $V(e, x)$ , such that for a closed-loop system (9)-(35)

$$V(e, x) > 0 \quad \text{and} \quad \frac{dV(e, x)}{dt} \leq 0 \quad (36) \quad \square$$

If the criteria imposed on the Lyapunov pair (36) are guaranteed for all  $x_0 \in X_0$ ,  $e_0 \in E_0$ ,  $u \in U$ ,  $r \in R$  and  $p \in P$ , the closed-loop system is robustly stable in  $X(X_0, U, P)$  and robust tracking is guaranteed in  $E(E_0, Y, R)$ . By explicitly deriving the total derivative for  $V(e, x)$ , the unknown feedback gains can be found to satisfy the sufficient conditions for stability. In particular, inequality  $\frac{dV(e, x)}{dt} \leq 0$  should be solved.

### 3.3. Implementation of Control Laws

The designed analog control laws can be straightforwardly implemented using operational amplifiers. Furthermore, arbitrary complexity filters can be implemented using operational amplifiers. If needed, microcontrollers can be used. Analog controllers are discretized using the sampling period  $T_s$ . For example, the feedback gains  $k_{dp}$  and  $k_{di}$  of the digital control law are found using the proportional, integral, and derivative coefficients of the analog PID control law as well as  $T_s$ . We have  $k_{dp} = k_p - 1/2 k_{di}$  and  $k_{di} = T_s k_i$ . The controller can be realized as  $u(kT_s) = k_p e(kT_s) + \frac{1}{2} k_i T_s \sum_{i=1}^k [e((i-1)T_s) + e(iT_s)]$ .

The proportional-integral controllers with the state feedbacks are implemented in the similar way.

## IV. CONTROL OF A HIGH-PERFORMANCE SERVO

We study pointing systems and hard drives. The requirements are to guarantee accurate and fast tracking and repositioning, eliminate steady-state positioning error (tracking error), attenuate disturbances, minimize the settling time, ensure robustness to parameter variations, etc. The specific features are the random disturbances due to non-uniformity, kinematics deviations, etc. Figure 3 illustrates the servo configuration and hardware test bed.

The actuator parameters are:  $r_a=7$  ohm,  $L_a=1\times 10^{-4}$  H,  $B_{\max}=0.7$  T,  $a=50$ ,  $N=100$ ;  $R_{\perp}=0.02$  m,  $l_{eq}=0.01$  m,  $B_m=5\times 10^{-8}$  N-m-sec/rad and  $J=23\times 10^{-7}$  kg-m<sup>2</sup>.

Using the tracking error  $e(t)$ , PID and proportional-integral with state feedback control laws are designed, examined and tested. The angular displacement  $\theta_r$  is measured by a high-accuracy sensor. The third-order notch filter attenuates the high-frequency noise.

Using the pole-placement approach, as well as Lyapunov theory, the feedback coefficients  $k_p$  and  $k_i$  of (26) are found. In general, the pole-placement concept may not ensure the desired eigenvalues despite coherent attempts to assign the adequate characteristic eigenvalues due to the control bounds. Using the quadratic function

$$V(e,x)=\frac{1}{2}(i_a^2+\omega_r^2+\theta_r^2+e^2), V(e,x)>0,$$

for the closed-loop system we apply the following inequality

$$\frac{dV(e,x)}{dt} \leq -q_e \|e\|^2, q_e=1.$$

The sufficient conditions are used to study the stability of the closed-loop system in  $X(X_0,U,P)$  and  $E(E_0,Y,R)$ . The PID control law (26) was experimentally verified. It is found that the assigned poles are not guaranteed due to the saturation and nonlinearities even for small  $r \in R$ . Furthermore, the system is sensitive to parameter variations and noise. The analog PI control algorithm is discretized and implemented using a microcontroller. It is found that digital controllers do not provide advantages, and that analog control schemes are the preferable solutions.

We tested a direct-drive servo with and without a restoring spring which is commonly used to ensure mechanical damping. The results are reported without the restoring spring. The output dynamics with different feedback gains  $k_p$  and  $k_i$  were observed. The reference is  $\theta_{ref}=0.349$  rad or  $\theta_r=20.2^\circ$ . As evident from Figure 6, the PI controller does not ensure the desired performance, such as, specified tracking accuracy, repositioning time, etc.

The desired tracking accuracy and other required performance quantities are achieved using the proportional-integral control with state feedback (23). We use the expanded state vectors, and

$$x^{sys}=[i_a \ \omega_r \ \theta_r]^T, x=[x^{sys} \ e]^T, z=[x \ u]^T.$$

Solving (20), from (22), the feedback matrices  $K_{F1}$  and  $K_{F2}$  are obtained. The control law (23) is implemented using analog ICs. The output dynamics are shown in Figures 6 for two different designs cases. In particular, changes of  $Q_z$  and  $G_z$  result in different  $K_{F1}$  and  $K_{F2}$ . The settling time and overshoot were minimized. A closed-loop servo-system operates at very high efficiency. High electromagnetic torque is developed to accurately reposition the pointer within minimum time. We conclude that optimal or near-optimal performance and capabilities are achieved

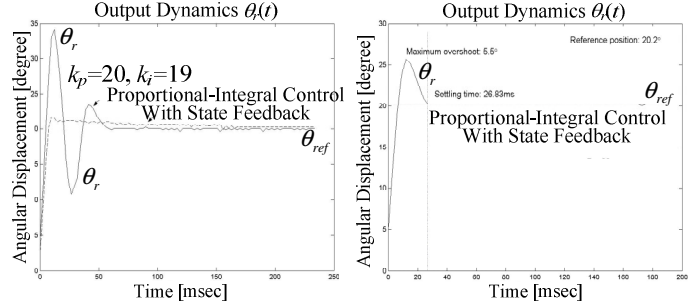


Figure 6. Output dynamics of the closed-loop servo with the bounded PI and proportional-integral controller with state feedback

## V. CONCLUSIONS

High-performance electromechanical systems, which are comprised from permanent-magnet actuators, sensors, PWM drivers and ICs, were studied. The major goal of this paper was to solve the motion control problem performing analysis and design of *minimal complexity* systems. Mathematical models were developed and used to design unbounded and bounded control laws. These control laws were implemented using operational amplifiers, ASICs and microcontrollers. Closed-loop system performance and capabilities (stability, accuracy, settling time and other) were examined. Near-optimal performance and exceptional capabilities were achieved and demonstrated. The reported results in the design of servo-systems are directly applied to other high-performance systems allowing one to achieve a spectrum of requirements and specifications commonly imposed on servo-drives and servomechanisms.

## REFERENCES

1. M. Abu-Khalaf and F. L. Lewis, "Nearly optimal HJB solution for constrained input systems using a neural network least-squares approach," *Proc. Conf. Decision and Control*, vol. 1, pp. 10-13, 2002.
2. D. S. Bernstein, "Optimal nonlinear, but continuous, feedback control of systems with saturating actuators," *Int. Journal Control.*, vol. 62, no. 5, pp. 1209-1216, 1995.
3. H. K. Khalil, *Nonlinear Systems*, Prentice Hall, Upper Saddle River, NJ, 1996.
4. D. Q. Mayne and W. R. Schroeder, "Nonlinear control of constrained linear systems," *Int. J. Control*, vol. 60, no. 5, pp. 1035-1043, 1994.
5. E. Sontag and H. J. Sussmann, "Nonsmooth control - Lyapunov functions," *Proc. Conf. Decision and Control*, New Orleans, LA, vol. 3, pp. 2799-2805, 1995.
6. S. E. Lyshevski, *MEMS and NEMS: Systems, Devices, and Structures*, CRC Press, Boca Raton, FL, 2002.
7. V. Giurgiutiu and S. E. Lyshevski, *Micromechatronics: Modeling, Analysis, and Design With MATLAB®*, CRC Press, Boca Raton, FL, 2009.
8. S. E. Lyshevski, *Control Systems Theory With Engineering Applications*, Birkhauser, Boston, MA, 2001.
9. S. E. Lyshevski, "Constrained optimization and control of nonlinear systems: New results in optimal control," *Proc. Conf. Decision and Control*, Kobe, Japan, vol. 1, pp. 541-546, 1996.
10. S. E. Lyshevski, "Optimization of nonlinear time-varying systems," *Proc. Conf. Decision and Control*, Tampa, FL, vol. 2, pp. 1798-1803, 1998.